biomass

MDPI

Article

From Hydrothermal Treatment to Pyrolysis: Kinetics, Thermodynamics, Evolved Gas Behavior, and Reaction Mechanism During Coupled Thermal Conversion of Chicken Manure

Akash Kumar [1,2,3], Lata Kumari [3], Moses Akintayo Aborisade [4], Belay Tafa Oba [5], Qiuxia Meng [2,6] and Qiang Zhang [6,7,*]

1 College of Resource & Environment, Shanxi Agricultural University, Taiyuan 030031, China
2 Institute of Eco-Environment and Industrial Technology, Shanxi Agricultural University, Taiyuan 030031, China
3 School of Chemical Engineering of Technology, Tianjin University, Tianjin 300350, China
4 School of Civil Engineering, Guangzhou University, Guangzhou 510006, China
5 College of Natural Science, Arba Minch University, Arba Minch P.O. Box 21, Ethiopia
6 Soil Health Laboratory in Shanxi Province, Taiyuan 030031, China
7 Shanxi Agricultural University, Taiyuan 030031, China
* Correspondence: zhangqiang0351@163.com; Tel.: +86-351-7639180

Abstract

Chicken manure represents a major agricultural waste stream with significant environmental risks if left unmanaged, yet its hydrothermally treated hydrochar (HCCM) holds promise as a renewable solid fuel. This study investigates the pyrolysis behavior, kinetics, thermodynamics, and gas evolution mechanism of HCCM using thermogravimetric analysis coupled with FTIR and mass spectrometry (TG-FTIR/TG-MS) at five heating rates (5–25 °C/min). TG-DTG results revealed a characteristic three-stage decomposition, with the main devolatilization occurring between 180 and 400 °C and a stable char residue of 22–27% remaining at 800 °C; DTG peaks shifted to higher temperatures and intensified with increasing heating rate, confirming a kinetically controlled process. Isoconversional analysis using the Flynn–Wall–Ozawa (FWO), Kissinger–Akahira–Sunose (KAS), and Starink (STK) methods; $R^2 > 0.98$ showed the apparent activation energy rising sharply from ~150 to over 320 kJ/mol with conversion, while consistently positive Gibbs free energy (130–210 kJ/mol) confirmed an endothermic, non-spontaneous reaction pathway. TG-FTIR and TG-MS identified CO_2, H_2O, carbonyl/amide fragments, and light hydrocarbons as dominant volatiles, with delayed H_2 release reflecting secondary aromatization and char condensation. These findings establish a mechanistic framework linking dehydration, decarboxylation, and aromatization reactions, supporting HCCM as a viable feedstock for sustainable energy recovery within a circular waste valorization strategy.

Keywords: chicken manure; hydrochar; pyrolysis; TG-FTIR/TG-MS; isoconversional kinetics; thermodynamic analysis

Check for updates

Academic Editor: Maurizio Volpe

Received: 17 July 2026
Revised: 27 August 2026
Accepted: 31 August 2026
Published: 1 September 2026

Copyright: © 2026 by the authors. Licensee MDPI, Basel, Switzerland. This article is an open access article distributed under the terms and conditions of the Creative Commons Attribution (CC BY) license.

1. Introduction

The amount of poultry produced globally has grown greatly during the last twenty years to meet increasing demands for low-cost animal proteins; it has been estimated that approximately 133.4 million tons of poultry were produced in 2020, and production is

expected to continue growing at an average rate each year [1]. Chicken meat and eggs are expected to be a significant portion of total world meat production during the next few years [2]. However, these large increases in poultry production also create massive amounts of manure and other waste as byproducts and represent a major risk to human and environmental health when not properly disposed of. Poultry waste byproducts are directly linked to emissions of NH_3, N_2O, and CH_4, which contribute to global greenhouse gas emissions. In addition, improper disposal of chicken manure has been shown to negatively affect animal and human health by degrading air and soil quality. Furthermore, increased levels of atmospheric ammonia due to improperly disposed of chicken manure can accelerate climate change. Due to the magnitude of the environmental impact of disposing of chicken manure, developing new environmentally friendly methods of producing valuable products from chicken manure has become a high priority for researchers.

Traditional methods of managing animal waste, i.e., directly applying or composting the waste on land and using anaerobic digesters to break down the organic matter, etc. provide some advantages but do little to eliminate concerns with respect to water quality due to potential losses of nitrogen and other nutrients from the soil via leaching, the potential for pathogens to survive during treatment, and the production of GHGs that will continue to be released until the organic material has decomposed to the point at which it no longer produces measurable levels of CO_2 [3,4]. Thus, there has been growing interest in thermochemical conversion technologies, e.g., pyrolysis and hydrothermal carbonization (HTC), that may serve as alternative ways of utilizing animal waste materials in order to reduce their volume, destroy pathogens associated with the waste material, and recover energy and/or carbon in a non-volatile solid form [5,6]. The HTC process is particularly suitable for use in processing wet biomass wastes like chicken manure because it utilizes liquid media at relatively mild temperatures (sub-critical temperature conditions typically found in the range of approximately 180–260 °C) and thus eliminates the need for drying the initial feedstock before undergoing thermal decomposition, producing a pathogen-free, carbon-rich solid product referred to as hydrochar through a combination of hydrolysis, dehydration, decarboxylation, polymerization, and aromatization reactions [7,8]. In addition to exhibiting similar characteristics of being free of pathogens, previous studies have indicated that hydrochars produced from manure-based feedstocks demonstrate significantly better fuel properties than those exhibited by the original biomass, e.g., higher fixed carbon content, increased HHV (higher heating value), and greater hydrophobicity leading to reduced degradation rates and increased storability, thereby providing a viable pathway for both solid fuel and soil amendment uses [9,10].

Although hydrochar presents many benefits as a low-cost biofuel source, it is difficult to use hydrochar as an advanced solid fuel without some form of additional thermal treatment; thus, pyrolysis represents a secondary method to continue the thermal densification of C, reduction in O-containing functional groups, and improvement of overall fuel properties compared to HTC alone [11,12]. As such, there is a need to fully understand the pyrolytic behavior of hydrochar generated from animal waste manures, including its thermal degradation characteristics, gaseous effluent generation patterns, kinetic behaviors, and thermodynamics, so that appropriate designs for commercial-scale pyrolytic reactors can be developed for HCM utilization. Due to its ability to determine mass loss characteristics of solid fuels under non-isothermal conditions, TG-DTG is currently the most commonly utilized experimental method for determining the pyrolysis behavior of solid fuels. However, when TG-DTG is combined online with FTIR spectroscopy (TG-FTIR) and mass spectrometry (TG-MS), the resulting experiment provides detailed information about both the gaseous products generated at each temperature range examined and their chemical structures, thereby offering mechanistic insight into the pyrolysis process that

is not obtainable using only TG-DTG data [13,14]. The development of pyrolysis reactor systems for HCM valorization will also require kinetic characterization of the pyrolysis behavior of HCM, typically performed through model-free isoconversional kinetic methods. The application of these methods allows for evaluation of the apparent activation energy as a function of the degree of conversion without prior knowledge of the specific reaction mechanisms involved in the pyrolysis process, whereas single heating rate models require determination of the activation energy based on assumed reaction mechanisms. These methods were recently recommended by the International Confederation for Thermal Analysis and Calorimetry (ICTAC) Kinetics Committee for studies involving solid-state thermal decomposition reactions [2,15]. Additional characterization of the pyrolysis behavior of HCM can be accomplished through application of thermodynamic parameters (ΔH, ΔS, ΔG), which can be determined via application of transition-state theory. Information regarding the energy requirements and feasibility of the pyrolysis process obtained from determination of these parameters is critical to the design and optimization of both reactor systems and processing operations [11,16].

The majority of research concerning hydrothermal carbonization and subsequent pyrolysis of several different manure types, including bovine, porcine, and avian manures, is relatively well-represented in the literature [7,9,15]; however, studies focusing on the pyrolytic behavior, multi-heating-rate kinetics, thermodynamics, and gas release mechanisms of chicken manure-derived hydrochar (HCCM) remain relatively rare. Because the primary compositional difference between chicken manure and other manure types is its markedly higher protein and nitrogen content [3], it remains unclear how this elevated nitrogen content influences the balance between decarboxylation/dehydration reactions and nitrogen release pathways (e.g., deamination and N-heterocycle formation) during devolatilization, and how this compositional difference is reflected in the conversion-dependent evolution of activation energy and thermodynamic parameters relative to lower-nitrogen manure-derived hydrochars. Addressing this gap requires not merely the application of multiple analytical techniques, but their integration into a single mechanistic framework capable of directly linking mass loss kinetics to the identity and timing of specific evolved gas species. The present study addresses this gap by combining multi-heating-rate TG-DTG analysis with isoconversional kinetics, transition-state-theory-based thermodynamics, and dual online evolved gas monitoring (TG-FTIR and TG-MS) to propose a mechanistic interpretation/framework for HCCM pyrolysis that explicitly accounts for its nitrogen-rich character, providing a basis for distinguishing its thermal decomposition behavior from that of other manure-derived hydrochars and thereby supporting the need for this individual study.

The goal of the current research is to provide a detailed characterization of the pyrolytic behavior of hydrochar obtained from chicken manure (HCCM), with an emphasis on the following aspects: (1) thermal decomposition characteristics of HCCM through TG-DTG analyses under different heating rates (five, namely 5, 10, 15, 20, and 25 °C/min); (2) evaluation of the apparent activation energy of pyrolysis in relation to the degree of conversion by applying the FWO, KAS, and Starink isoconversional methods; (3) thermodynamic parameters that define the pyrolytic process (ΔH, ΔS, ΔG); (4) identification and evolution patterns of gaseous compounds produced during the pyrolytic degradation of HCCM through TG-FTIR and TG-MS techniques; and (5) proposal of a reaction scheme that integrates all previous experimental data. This research project is based on the hypothesis that it will provide basic information and mechanistic insights for designing and optimizing technologies to pyrolyze chicken manure into value-added products such as sustainable solid fuel or carbonaceous material.

2. Materials and Methods

2.1. Feedstock Collection and Preparation

The hydrochar derived from chicken manure (HCCM) used in this study was prepared at Tianjin University, Tianjin, China. Hydrothermal treatment was conducted in a 600 mL hydrothermal reactor (HT–250 J0, HTLAB, Beijing, China). In each run, 20 g of raw chicken manure was loaded into the reactor vessel along with 200 mL of deionized water (solid-to-liquid ratio of 1:10), ensuring thorough mixing. Following closure of the reactor, the system was purged with argon to establish an oxygen-free atmosphere. The solid–water mixture was agitated at a rotational speed of 150 rpm and heated to a target temperature of 180 °C, with a holding time of 30 min following attainment of the target temperature. The reactor pressure was maintained autogenously by the water vapor pressure generated at the operating temperature. Upon completion of the reaction, the reactor was allowed to cool gradually to ambient room temperature. The resulting solid–liquid mixture was separated by vacuum filtration, and the recovered hydrochar was oven-dried at 105 °C for 24 h prior to use in the pyrolysis experiments.

The hydrochar yield was calculated as:

$$Yield\ (wt.\%) = \frac{mass\ of\ hydrochar}{mass\ of\ dry\ raw\ feedstock} \times 100\% \quad (1)$$

The hydrochar yield for HCCM, prepared at 180 °C with a 30 min residence time (solid-to-liquid ratio of 1:10), was 30.35 ± 1.93 wt.%.

Before thermal analysis, the sample was ground/sieved to a particle size of less than 0.15 mm in diameter to ensure homogeneity and minimize heat and mass transfer limitations during pyrolysis experiments. This process is a common approach for preparing samples for thermal decomposition of solid organic materials while minimizing potential heat and mass transfer effects on thermal decomposition rates. Samples of each of these uniformly sized powders were placed in separate containers and stored in a desiccator before testing to prevent water reabsorption.

2.2. Proximate and Ultimate Analysis

Proximate analysis (ASTM D3172-D3175) (ASTM International, 2013) was conducted on the feedstocks to determine their moisture, volatile matter, ash, and fixed carbon content through standard methods. Higher heating values (HHV's) were determined using an oxygen bomb calorimeter. The elemental (ultimate) composition of carbon, hydrogen, nitrogen, sulfur, as well as the oxygen content, was obtained from the CHNS elemental analyzer. As such, these results are consistent with standard ultimate analysis practices (e.g., ASTM D3176 and D5373) (ASTM International, 2015); the oxygen content is therefore represented by the mass balance difference. The resultant proximate and ultimate data (see Table 1) were utilized to evaluate the pyrolytic behavior of each of the three feedstocks and to describe the observed differences in their decomposition processes.

2.3. Instrumentation

Non-isothermal TGA tests were run on simultaneous thermal analyzers (STA449F5 and STA8000, NETZSCH, Selb, Germany), and evolved gas analysis was performed by coupling a Frontier FTIR (Fourier transform infrared spectroscopy) (Perkin Elmer, Shelton, CT, USA) with the STA. A smaller number of volatile compounds was also analyzed using GC/MS (gas chromatography/mass spectrometry) (Clarus SQ8, Perkin Elmer, USA). The calorific value and elemental composition were determined using an oxygen bomb calorimeter (SHR-15B, Nanjing Sangli Electronic Equipment Factory, Nanjing, China), and an elemental analyzer (Vario EL Cube, Elementar, Hesse, Germany), respectively.

Table 1. Proximate and ultimate analysis of raw chicken manure (CM) and chicken manure hydrochar (HCCM).

Sample	Proximate Analysis (wt.%)				HHV ($MJ \cdot kg^{-1}$)	Ultimate/Elemental Analysis (wt.%, Dry Basis)					Atomic Ratios (Dry, Ash-Included Basis)		
	M (ar, %)	VM (d, %)	Ash (d, %)	FC* (d, %)		C	H	O *	N	S	H/C	N/C	O/C
CM (raw)	3.51	61.04	27.22	8.26	17.3	42.13	6.19	21.54	3.83	0.06	1.75	0.078	0.38
HCCM	–	63.27	29.27	7.46	22.25	46.27	7.12	16.18	1.08	0.08	1.83	0.02	0.26

FC* = 100 − (M + A + VM); *: by difference.

2.4. Non-Isothermal Pyrolysis (TG-DTG) Experiments

Approximately 8.0 ± 0.5 mg of each sample subjected to some form of pretreatment was placed in an Al_2O_3 crucible, then heated to 800 °C in a high-purity nitrogen gas flow environment (20 mL/min), with temperatures ranging from 35 to 800 °C. The pyrolysis process (non-oxidative) was used during this temperature range to ensure that no oxidation would occur during the process. Five different heating rates were utilized to analyze the samples as part of the multi-heating-rate analysis. These heating rates included: 5 °C/min, 10 °C/min, 15 °C/min, 20 °C/min and 25 °C/min. This multi-heating-rate analysis is necessary to provide sufficient information for kinetic models. Prior to measuring each sample, a blank run was conducted using the same parameters so that any variation due to instrumental drift or buoyancy could be accounted for.

2.5. Coupled TG-FTIR-GC/MS Analysis of Volatile Products

Pyrolytic volatile products were identified as gaseous or condensable species using an online TG-FTIR-GC/MS setup. The experimental setup was similar to those previously used for online monitoring of real-time volatile release from biomass and waste samples through evolved gas analysis (EGA). The thermal analyzer utilized to pyrolyze the approximately 8.0 ± 0.5 mg of HCCM sample had a constant heating rate of 10 °C/min. This allowed for the entire temperature range (35–800 °C) to be studied. Pyrolysis occurred under a nitrogen flow of 20 mL/min. Spectral data were obtained from the evolving gas stream using the FTIR spectrometer. A heated transfer tube connected the thermal analyzer to the FTIR spectrometer. This connection permitted continuous sampling of the gas stream so that real-time spectral information could be collected by the FTIR (400–4000 cm^{-1}, 4 cm^{-1} resolution). Volatile compounds generated at the maximum weight loss rate (270 °C) were also extracted from the thermal analyzer and analyzed using GC/MS. This provided compound-specific identification of the volatile components. All TG-DTG, TG-FTIR, and TG-MS analyses were performed in triplicate for each heating rate to verify data reproducibility. Given the continuous, high-resolution nature of the mass loss and evolved gas curves, a single representative replicate is shown in each figure for visual clarity, while the reproducibility of the key characteristic parameters (onset temperature, peak decomposition temperature, maximum decomposition rate, and final residual mass) is reported as mean ± standard deviation across the three replicates in Table S1 (Supplementary Material).

2.6. Pyrolysis Kinetic Modeling

To determine the perceived activation energy (E_a) of pyrolytic decomposition, the FWO, KAS, and STK models were applied. The governing equations are:

The pyrolytic kinetics were determined based on the thermogravimetric data, thus:

$$\frac{d\alpha}{dt} = k(T).f(\alpha) \quad (2)$$

The symbol k(T) denotes the reaction rate constant, while f(α) denotes the reaction mechanism function. The variables T, α, and t correspond to the temperature, the extent of conversion, and time, respectively.

The conversion degree (α) can be specified as follows:

$$\alpha = \frac{m_o - m_t}{m_o - m_f} \tag{3}$$

where m_t is the sample mass at time t, and m_o and m_f are the initial and final masses, respectively.

The conversion rate is then expressed as:

$$\frac{d\alpha}{dt} = kf(\alpha) \tag{4}$$

where k follows the Arrhenius equation, which accounts for the temperature dependence, and f(α) represents the reaction mechanism model. By introducing the heating rate β = dT/dt, the equation can be written as:

$$k = A^{-\frac{Ea}{RT}} \tag{5}$$

$$\beta\frac{d\alpha}{dT} = Ae^{-\frac{Ea}{RT}}f(\alpha) \tag{6}$$

The integrated form of Equation (5) is given by:

$$G(\alpha) = \int_0^{\alpha} \frac{d\alpha}{f(\alpha)} = \int_0^{T} \left(\frac{A}{\beta}\right) \exp\left(\frac{-E}{RT}\right) dT = \left(\frac{AE}{\beta R}\right) p(u) \tag{7}$$

Isoconversional Methods

The activation energy (E_a) was estimated using three model-free isoconversional methods: FWO, KAS, and STK. By substituting $u = E/RT$ into the fundamental kinetic equation, different approximations for the temperature integral $P(u)$ allow for the determination of E_a without assuming a reaction model $f(\alpha)$. Using Doyle's approximation:

$$\ln p(u) = -2.315 - 0.4567\frac{E}{RT} \tag{8}$$

Leads to the following equations for the FWO, STK, and KAS methods, respectively:

$$\ln\beta = \ln\left[\frac{AEa}{RG(\alpha)}\right] - 2.315 - 0.4567\left(\frac{Ea}{RT}\right) \tag{9}$$

$$\ln\left(\frac{\beta}{T^2}\right) = \ln\left[\frac{AE\alpha}{RG(\alpha)}\right] - \frac{Ea}{RT} \tag{10}$$

$$\ln\left(\frac{\beta}{T^{1.92}}\right) = Cs - 1.0008\frac{Ea}{RT} \tag{11}$$

2.7. Thermodynamic Analysis

The thermodynamic characteristics of pyrolytic decomposition, the pre-exponential factor (A), the activation enthalpy (ΔH), the Gibbs free energy of activation (ΔG), and the activation entropy (ΔS), were determined from the activation energies that were obtained

using the FWO, KAS, and STK isoconversional models. The following standard equations were used to calculate the thermodynamic properties from the activation energies:

$$Enthalpy\ changes\ \Delta H = E_a - RT_m \tag{12}$$

$$Entropy\ changes\ \Delta S = \frac{\Delta H - \Delta G}{T_m} \tag{13}$$

$$Gibbs\ Free\ Energy\ \Delta G = E_a + RT_m \ln\left(\frac{K_B T_m}{hA}\right) \tag{14}$$

where E_a is the apparent activation energy (kJ·mol^{-1}) obtained from the FWO, KAS, or STK isoconversional method at a given conversion (α); R is the universal gas constant (8.314 J·mol^{-1}·K^{-1}); T_m is the peak (DTG maximum) temperature (K) corresponding to the maximum decomposition rate at each heating rate; A is the pre-exponential factor (min^{-1}) derived from the corresponding isoconversional method; kB is the Boltzmann constant (1.381×10^{-23} J·K^{-1}); and h is Planck's constant (6.626×10^{-34} J·s). ΔH, ΔS, and ΔG are expressed in kJ·mol^{-1}, J·mol^{-1}·K^{-1}, and kJ·mol^{-1}, respectively. Because the calculation of ΔS (Equation (5)) requires the corresponding ΔG value, ΔG (Equation (6)) was calculated directly from E_a, T_m, and A prior to ΔS.

3. Results and Discussion

3.1. Atomic H/C and O/C Ratio and Proximate and Ultimate Analysis of Raw Chicken Manure and HCCM

To further characterize the extent of hydrothermally induced structural change, atomic H/C, N/C, and O/C ratios were calculated from the elemental composition (Table 1) using the following formula:

$$Atomic\ ratio = \frac{wt.\%\ element/atomic\ weight\ of\ element}{wt.\%\ C/12.01} \tag{15}$$

using standard atomic weights (C = 12.01, H = 1.008, N = 14.01, O = 16.00 g/mol). The resulting values are summarized in Table 1: the O/C ratio decreased from 0.38 (CM) to 0.26 (HCCM); the H/C ratio increased from 1.75 (CM) to 1.83 (HCCM); and the N/C ratio decreased from 0.078 (CM) to 0.020 (HCCM).

To further quantify the nitrogen loss reflected in the N/C ratio, a solid-phase nitrogen mass balance was performed (basis: 100 g dry raw feedstock):

$$N_{raw} = 100\ g \times 3.83\% = 3.83\ g\ N$$

$$m_{hydrochar} = 30.35\ g$$

$$N_{hydrochar} = 30.35\ g \times 1.08\% = 0.328\ g\ N$$

$$N\ retained\ in\ hydrochar = \frac{0.328}{3.83} \times 100 = 8.6\%$$

$$N\ removed\ from\ solid\ phase = 100 - 8.6 = 91.4\%$$

However, the that atomic O/C ratios are a bulk elemental indicator derived from CHNS elemental analysis and ash content; while their direction of change is consistent with deoxygenation, this bulk measurement cannot, on its own, confirm the specific molecular removal pathway (e.g., preferential loss of hydroxyl versus carboxyl groups) without complementary molecular-level characterization (e.g., solid-state ^{13}C NMR or XPS), which was outside the scope of the present study.

The slight increase in H/C ratio is interpreted cautiously as being consistent with, rather than direct proof of, comparatively greater retention of aliphatic character in HCCM relative to more severely treated hydrochars reported elsewhere. This interpretation is supported only indirectly, by the co-occurring prominence of light aliphatic hydrocarbon fragments (CH_3, C_2H_2) in the TG-MS evolved gas profile (Section 3.6). Atomic H/C ratios and TG-MS ion-current fragment data do not, individually or in combination, constitute direct structural confirmation of aliphatic chain retention, and should instead be regarded as complementary, consistent lines of indirect evidence supporting a plausible rather than demonstrated interpretation.

The marked decrease in N/C ratio is directly supported by the solid-phase nitrogen mass balance above, which indicates that only 8.6% of the original feedstock nitrogen was retained in HCCM, with the remaining 91.4% presumed redistributed to the aqueous HTC process water (assuming negligible gas-phase nitrogen loss at this moderate HTC temperature of 180 °C). This mass balance result provides direct, quantitative support for the N/C ratio trend, in contrast to the more indirect, literature-based reasoning applied above to the H/C and O/C interpretations.

The solid-phase nitrogen mass balance above indicates that approximately 91.4% of the original feedstock nitrogen was not retained in HCCM, most likely redistributed into the aqueous HTC process water, assuming negligible gas-phase nitrogen loss at the moderate HTC temperature used in this study (180 °C). This is consistent with, though not independently confirmed by, the well-documented behavior of nitrogen during hydrothermal carbonization of manure feedstocks, whereby labile nitrogen species including ammonium, soluble proteins, and amino compounds are preferentially solubilized into the aqueous process water rather than retained in the solid hydrochar. Poultry litter HTC process water has been reported to contain substantial dissolved nitrogen, supporting the plausibility of this redistribution pathway [17]. We note, however, that process water nitrogen concentration was not directly measured in the present study; therefore, while our solid-phase mass balance demonstrates that nitrogen was not retained in HCCM, its presumed fate in the aqueous phase (rather than partial loss to the gas phase) remains a literature-supported interpretation rather than a directly confirmed result. The residual nitrogen retained in HCCM (1.08 wt.%) likely comprises nitrogen bound within more condensed, less hydrolyzable structures (e.g., heterocyclic or amide-bound nitrogen) that resist solubilization under the hydrothermal conditions applied (180 °C, 30 min).

Comparison of the proximate and ultimate analyses of CM and HCCM (Table 1) reveals the characteristic compositional changes induced by hydrothermal treatment (180 °C, 30 min, solid-to-liquid ratio of 1:10). Ash content increased from 27.22% to 29.27% and carbon content rose from 42.13% to 46.27%, reflecting the combined effects of mass loss via dehydration and decarboxylation and the relative concentration of inorganic and carbonaceous fractions during hydrothermal conversion. This concentration effect is consistent with the measured hydrochar yield (30.35 ± 1.93%, Section 2.1). Correspondingly, oxygen content decreased from 21.54% to 16.18%, and the atomic O/C ratio declined from 0.38 to 0.26, consistent with the preferential removal of oxygen-containing functional groups as H_2O and CO_2 during hydrothermal dehydration and decarboxylation reactions [8,10]. Nitrogen content decreased substantially, from 3.83% to 1.08%, indicating solubilization of labile protein- and amino-acid-derived nitrogen into the aqueous HTC process water, consistent with reported nitrogen partitioning behavior during hydrothermal treatment of manure feedstocks [17,18].

These compositional changes are directly reflected in the thermal decomposition behavior of HCCM observed by TG-DTG (Section 3.2). The reduced oxygen content and lower proportion of labile, oxygen-rich functional groups in HCCM relative to raw

CM are consistent with the absence of a distinct low-temperature hemicellulose-related shoulder in the HCCM DTG curves, since these oxygen-rich, thermally labile structures are largely removed during the preceding hydrothermal step. The elevated ash content of HCCM is likewise consistent with the substantial solid residue (22–27%) retained at 800 °C across all heating rates, as the concentrated inorganic mineral fraction remains largely unreacted throughout pyrolysis; this mineral content, which includes alkali and alkaline earth species known to catalytically promote biomass devolatilization, may also contribute to the comparatively lower DTG peak temperature (250–270 °C) observed for HCCM relative to hydrochars produced under different hydrothermal severities [10]. The comparatively higher carbon content and lower oxygen content of HCCM relative to typical raw lignocellulosic biomass are further consistent with its improved heating value (17.3 → 22.25 MJ/kg) and with the dominance of decarboxylation/decarbonylation as a primary devolatilization pathway identified by TG-FTIR and TG-MS (Sections 3.5 and 3.6).

3.2. Thermogravimetric (TG–DTG) Analysis of HCCM at Different Heating Rates

The thermal decomposition behavior of the hydrochar obtained from chicken manure (HCCM) was investigated using TG-FTIR in a non-isothermal pyrolysis mode at five different heating rates (5, 10, 15, 20, and 25 °C/min). TG and DTG profiles were determined as shown in Figure 1. Overall, it is evident that for all five heating rates, the decomposition of HCCM occurs through three stages of mass loss, typically representative of LCMs (lignocellulosic materials) and CMs (carbonaceous materials) derived from biomass and organic waste such as animal manures [19,20]. Stage one represents a very small weight loss due to the desorption of free or weakly adsorbed water from the hydrochar prior to the onset of significant pyrolytic decomposition (typically < 100 °C). However, in the case of the hydrochar samples studied here, a marginal weight loss is evident throughout this range. Stage two, representing the major pyrolytic decomposition event (typically between approximately 180 and 400 °C), accounts for the majority of the total weight loss and results in the observation of a high DTG peak value for each of the heating rates used. This stage can be associated with the thermal degradation of the remaining protein/starch/hemicellulose components present in the hydrochar post-HTC treatment and/or residual cellulose [20]. A third, final stage representing a more rapid but still relatively slow mass loss event extends from approximately 400 °C to 800 °C and corresponds to the continued thermal decomposition of more refractory aromatic (and possibly lignin-like) residues left behind upon completion of the initial devolatilization process. In all cases, this final stage resulted in a residual solid content of about 22–27 wt.% at 800 °C. This multi-stage decomposition profile parallels that observed previously in other HTC-treated manure-based hydrocars and biochars, where thermal decomposition is characterized by drying, devolatilization, and char/carbonization stages [21,22].

Increasing the heating rate from 5 to 25 °C/min produced noticeable changes in the shape and magnitude of the DTG curves for the HCCM samples. These included: (i) an upward shift in T_{max} (the peak decomposition temperature) as the heating rate increased; and (ii) A substantial increase in the maximum rate of mass loss (DTG_intensity max) with increasing heating rate, i.e., an increase from −4 wt.%/min at 5 °C/min to greater than −20 wt.%/min at 25 °C/min. Both effects have been extensively documented for untreated and hydrothermally treated biomass pyrolysates and are usually interpreted in terms of a combination of heat transfer limitation factors and reaction kinetics. For example, when heating rates are increased significantly above those achievable during static laboratory-scale experiments, a larger thermal gradient arises between the surface and center of the sample, resulting in a lagging effect in heating within the central regions of the sample. As a result, T_{max} values are displaced toward higher temperatures [22]. Similar

observations regarding the influence of heating rate on DTG peak position have also been made by others working on kinetic models for HTC-treated hydrochar pyrolysis, where they attribute similar effects to both heat/mass transfer-related factors and to inherent devolatilization kinetics [23].

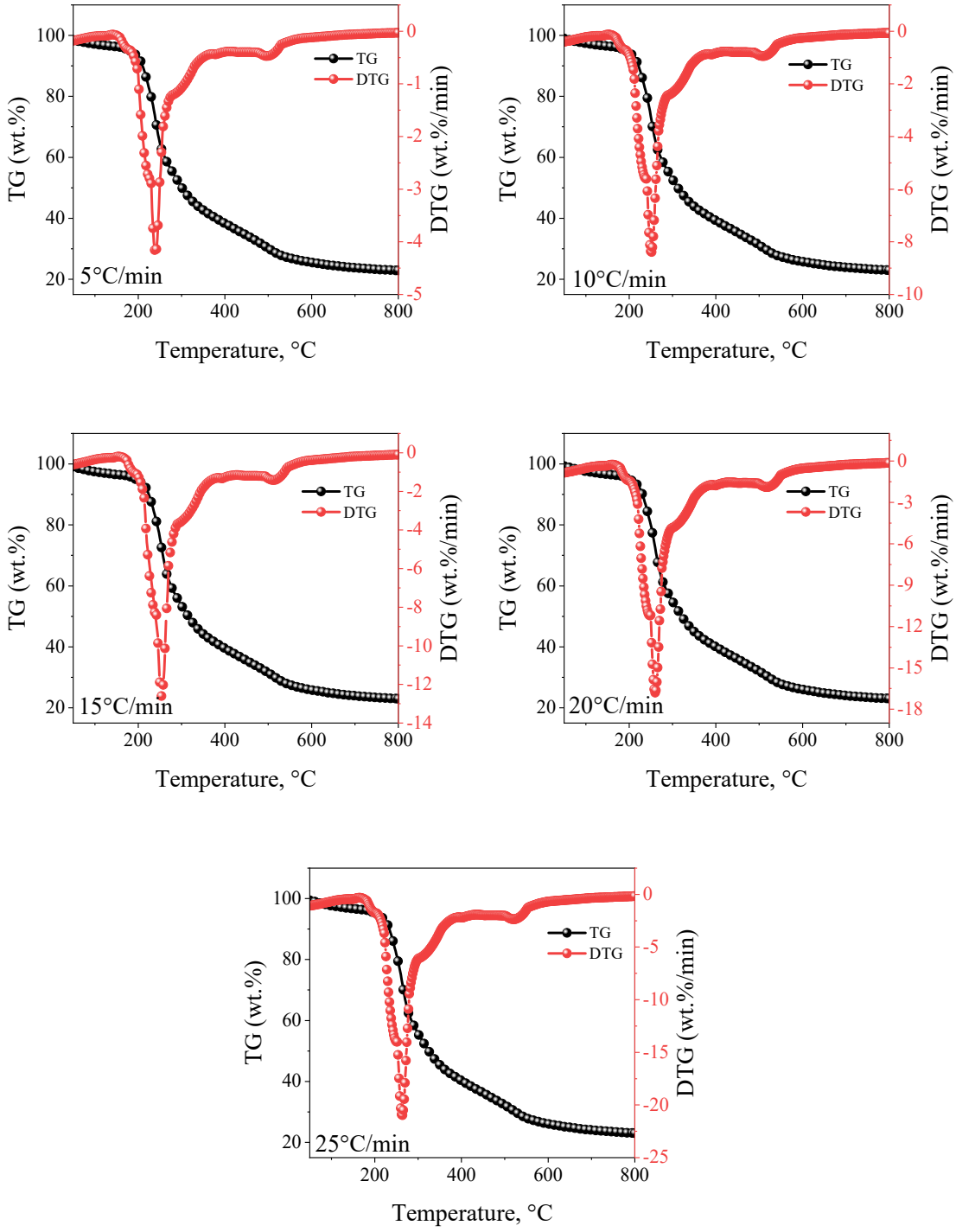


Figure 1. TG and DTG profiles of HCCM pyrolysis at different heating rates.

Comparison with related manure-derived materials. The overall form and temperature range of the results for HCCM were similar to those reported previously by other researchers studying chicken manure and its resultant char through TG. Non-hydrothermally treated chicken manure was shown to be within a similar temperature range for devolatilization onset during multiple heating rates [24]. It was also reported to exhibit distinct dehy-

dration, preheating, pyrolysis, carbonization, and secondary pyrolysis stages, respectively, when studied using TG-DTG methods at heating rates of 5–20 °C/min under an inert atmosphere [19]. A lack of a clear, low-temperature hemicellulose shoulder in the HCCM DTG curves relative to what would typically appear in raw lignocellulosic biomass is consistent with reports showing that hydrothermal carbonization treatment can remove or dissolve large portions of the hemicellulose fraction before pyrolysis [21].

In total, the systematic variation in T_{max} with increasing heating rate, along with the corresponding increases in maximum decomposition rate, indicates that the pyrolysis of HCCM is a kinetically controlled process that will be suitable for future use with model-free (isoconversional) kinetic models, including KAS, FWO, or STK analysis, all of which rely upon multi-heating-rate TG-DTG data of the exact same format as those used in this study [24].

3.3. Isoconversional Kinetic Analysis of HCCM Pyrolysis

To determine the apparent activation energy (E_a) for pyrolysis of HCCM without assuming a specific reaction mechanism, three model-free methods were applied to TG data collected at different heating rates: Flynn–Wall–Ozawa (FWO), Kissinger–Akahira–Sunose (KAS), and Starink (STK). These methods are recommended by the ICTAC Kinetics Committee for the degradation of solids because they allow activation energy to be evaluated as a function of conversion (α) without selection of a reaction model. The Starink method has been evaluated by the ICTAC Committee, and the Committee concluded that the Starink approach is among the most reliable integral isoconversional methods for estimating apparent kinetic parameters [2]. For each method, linear plots were constructed at degrees of conversion from α = 0.10 to 0.85: ln β versus 1/T for FWO, ln β/T^2 versus 1/T for KAS, and ln(β/T1.9) versus 1/T for STK, where β is the heating rate, and T is the absolute temperature corresponding to a given α at each heating rate (Figure 2). Activation energies at each conversion level were obtained from the slopes of the corresponding regression lines. All three methods produced good linear fits across the conversion range investigated; generally, correlation coefficients (R^2) exceeded 0.983 for most α values but dropped slightly around α between 0.75 and 0.8 before recovering at higher conversion levels. Behavior like this has been reported in other kinetic studies of pyrolysis of manure and biomass and is usually interpreted as a signature of a transition between dominant mechanisms or overlapping decomposition steps rather than as a failure of the model itself because profiles obtained from KAS, FWO, Starink, and Vyazovkin methods are generally very similar, while Friedman method values can diverge somewhat because underlying approximations differ [15].

The apparent activation energies for HCCM pyrolysis were found to increase monotonically with conversion levels for all three methods. Specifically, they ranged from approximately 150 KJ/mol at α = 0.10 to over 320 KJ/mol at α = 0.85. Additionally, the three kinetic methods used (FWO, KAS, and STK) provided very similar E_a values at each conversion level, which was expected due to all three being integral isoconversional methods derived from equivalent temperature-integral approximations that tend to converge closely with one another. Therefore, the high degree of agreement between these multiple isoconversional methods provides confidence in the reliability of the calculated kinetic parameters, since agreement amongst multiple isoconversional methods is generally accepted as an indicator of robustness and consistency within a kinetic description of decomposition processes [15].

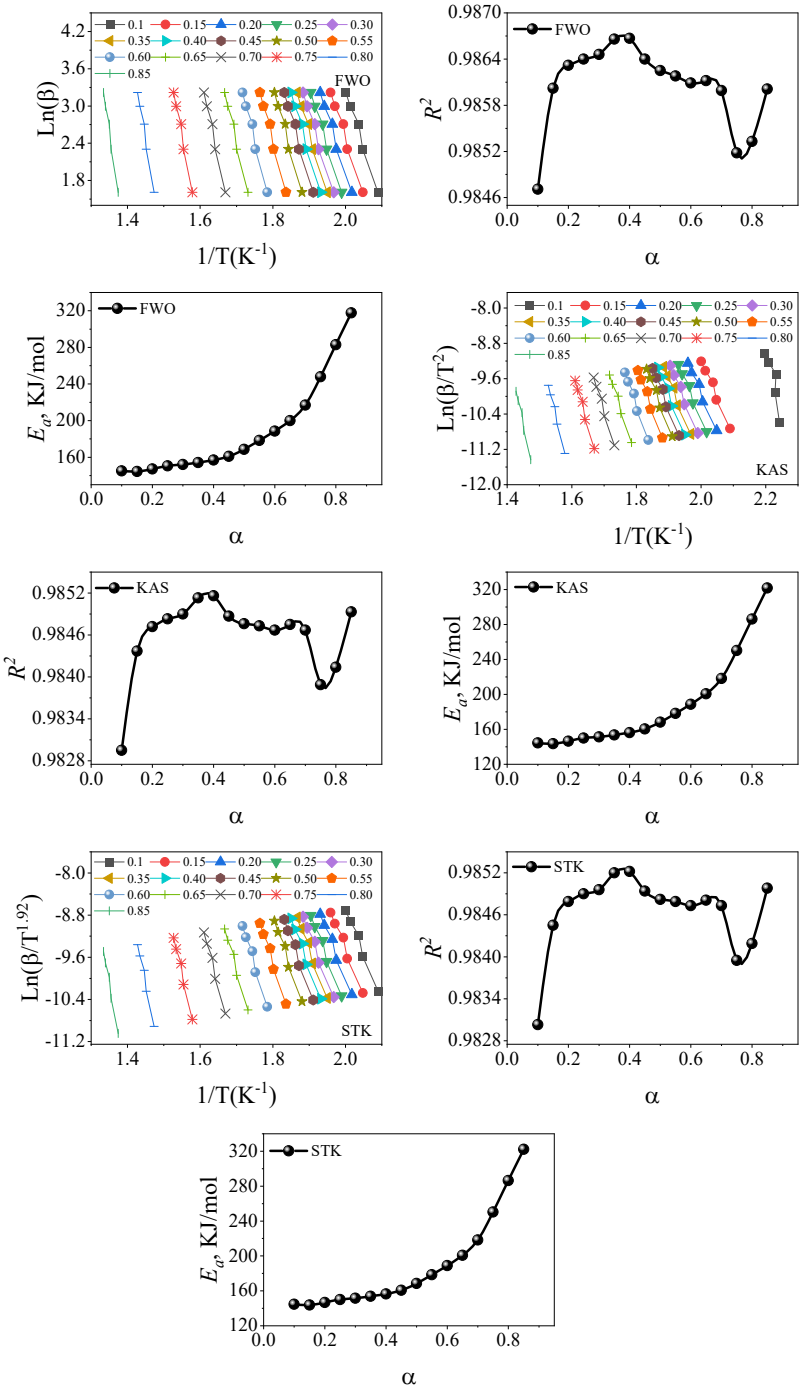


Figure 2. Isoconversional kinetic analysis of HCCM pyrolysis using FWO, KAS, and STK models.

In addition to providing a method for assessing the kinetics of hydrochar decomposition, the progressive rise in E_a values indicates that HCCM pyrolysis does not involve a single simple reaction mechanism but rather a series of parallel and/or interacting reactions of increasing complexity as decomposition proceeds. For low conversion values ($\alpha < 0.30$), the lower E_a values (approximately 150–180 KJ/mol) represented by the relatively stable E_a values indicate the presence of more labile residual carbohydrate- and protein-derived fractions retained in the hydrochar after hydrothermal carbonization. Conversely, the sharp increases in E_a toward values of 300–320 KJ/mol observed at higher conversion levels ($\alpha > 0.60$–0.70) reflect the greater thermal stability of the more condensed, cross-like, and aromatic char structures formed during hydrothermal carbonization. Therefore, these char structures require substantially more energy to break down than the less complex hydro-

carbon fractions present in the initial hydrochar. Overall, this trend is broadly consistent with other manure-derived feedstocks that have been analyzed using various isoconversional methods [25] and with studies examining cattle manure pyrolysis, where average E_a values obtained across FWO, KAS, Starink, and Friedman methods ranged between 158 and 162 KJ/mol [26]. The magnitude and conversion dependence of E_a obtained for HCCM also fall within the broader range reported for lignocellulosic and agro-industrial biomass wastes analyzed using the above-named kinetic methods [15] and are comparable to hydrochar-specific kinetic studies examining hydrochars derived from organic waste blends via HTC using KAS, FWO, and Starink methods [27].

To further address whether the high E_a values obtained at high conversion (up to ~320 kJ/mol) reflect a genuine structural origin rather than a methodological artifact, it is useful to compare these results with hydrochar- and manure-specific literature reporting similarly elevated activation energies at high conversion. A thermogravimetric study comparing manure and crop residue-derived biochars, including a direct rice bran–chicken manure comparison, reported that E_a increased steeply at $\alpha > 0.65$ and attributed this sharp rise specifically to the higher mineral (ash) content of manure-derived feedstocks relative to lignocellulosic residues [28]. Given that HCCM likewise possesses a substantial ash content (29.27 wt.%, Table 1), a comparable mineral-catalyzed effect on the high-conversion decomposition pathway is plausible. Furthermore, isoconversional analysis of lignin, the most thermally recalcitrant and aromatic biomass component, has reported E_a values rising from 174 to 322 kJ/mol across a similar conversion range (α = 0.05–0.79), closely matching the magnitude observed here for HCCM at high conversion [29]. Because hydrothermal carbonization is known to promote polymerization and aromatization of the solid product [8], the condensed, lignin-like aromatic structures formed during HTC pretreatment provide a structurally consistent explanation for the elevated E_a observed at high conversion in the present study. Regarding possible methodological effects, we note that isoconversional activation energies reported across the biomass and hydrochar pyrolysis literature span an especially wide range (approximately 10–660 kJ/mol) depending on feedstock and conversion level [15], indicating that values in the 300 kJ/mol range, while high, are not unprecedented or inherently indicative of a calculation artifact. Moreover, at high conversion, the DTG signal becomes smaller in magnitude and more susceptible to baseline noise, which can introduce some scatter into isoconversional fits; however, the close agreement observed here between the three independent isoconversional methods (FWO, KAS, and STK), together with consistently high R^2 values, argues against a purely methodological origin. However, based on the present dataset, we cannot conclusively distinguish whether the elevated E_a values at high conversion arise predominantly from the mineral/ash-catalyzed effect suggested by comparison with manure-specific literature [28], from the formation of condensed, lignin-like aromatic char structures during hydrothermal pretreatment [8,29], or most likely from a combined contribution of both mechanisms acting concurrently. We therefore present these as co-existing, non-mutually exclusive explanations rather than favoring either mechanism as definitively established. Isolating their individual contributions would require additional targeted experiments (e.g., pyrolysis of demineralized/acid-washed HCCM to remove catalytically active mineral species while preserving the char's aromatic structure), which are beyond the scope of the present study and are identified here as a direction for future work.

Overall, the good agreement among all three models (FWO, KAS, and STK), along with consistent and good-to-excellent R^2 values, supports the validity of the isoconversional approach for describing HCCM pyrolysis kinetics. Further, it confirms that HCCM undergoes a multi-stage reaction whose apparent activation energy increases with the degree of conversion.

3.4. Thermodynamic Analysis of HCCM Pyrolysis

To better understand the thermal aspects of HCCM pyrolysis, the thermodynamic activation parameters, i.e., the changes in enthalpy (ΔH), entropy (ΔS), and Gibbs free energy (ΔG), were calculated from the isoconversional activation energies (E_a) derived by means of the FWO, KAS, and STK methods, using the basic equations of the transition-state (activated complex) theory. This method has become commonly accepted for supplementing isoconversional kinetic analysis because determining ΔG, ΔH, and ΔS from E_a and the pre-exponential factor is an essential goal for understanding the mechanism of pyrolytic reactions and the energy intensity and thermochemical feasibility of biomass conversion processes [11]. It is also important to note that these parameters define the transition from reactants to activated complexes as opposed to describing the entire reactant-to-product transformation, a critical distinction that needs to be made when interpreting results correctly [30].

As illustrated in Figure 3, ΔH exhibited nearly the same behavior as E_a for each of the three methods (FWO, KAS, and STK); therefore, it increased from about 135–140 KJ/mol at lower conversions (i.e., $\alpha = 0.10$) to almost 310–320 KJ/mol at higher conversions (i.e., $\alpha = 0.85$). Since ΔH is proportional to E_a via $\Delta H = E_a - RT$, the approximate agreement in value and similar trend of ΔH and E_a indicate a relatively small barrier for the separation of reactants from the activated complexes, and that the reaction exhibits an endothermic nature over the entire conversion range; this agrees with general observations based on the literature that a slight difference between E_a and ΔH may be indicative of a thermodynamically advantageous situation for proceeding [31].

The ΔS values were relatively stable at low to intermediate conversions (e.g., $\alpha < 0.50$) before increasing significantly with higher conversions; they reached approximately 140–150 KJ/mol at $\alpha = 0.85$ for all three methods. Near-zero or negative values of ΔS at low conversions suggest that the activated complexes produced during the initial stages of HCCM decomposition are structurally very close to their parent materials; this represents a system near thermodynamic equilibrium. Larger positive values of ΔS represent a more disordered activated state and, consequently, a system farther away from equilibrium [32]. The marked rise in ΔS values at high conversions indicates an increasingly large breakdown of the complex crosslinked char structure into a greater number of smaller disordered fragments and gas-phase products; this is typically characteristic of a faster reaction pathway in the latter stages of solid-state decomposition [33].

Unlike ΔH and ΔS, ΔG only increases slightly and continually with conversion, from approximately 130 kJ/mol at $\alpha = 0.10$ to about 200–210 kJ/mol at $\alpha = 0.85$ across all three methods (FWO, KAS, and STK). The relatively narrow range of ΔG, compared with the larger variations in ΔH and E_a, reflects the counterbalancing effect of the simultaneously increasing ΔS term. It is important to note that the calculated ΔG values represent the Gibbs free energy of activation (ΔG), which describes the energy barrier associated with formation of the activated complex from reactants, rather than the thermodynamic spontaneity of the overall pyrolysis reaction [30]. The consistently positive and increasing ΔG across the conversion range therefore reflects a progressively more energy-demanding transition state and increased resistance to decomposition at higher conversion levels, rather than evidence that HCCM pyrolysis is thermodynamically non-spontaneous as an overall process.

All of the ΔH, ΔS, and ΔG profiles produced by the FWO, KAS, and STK methods were in general agreement at each conversion level, similar to the agreement found in the E_a results. Agreement among the three methods further supports the validity of the thermodynamic data generated and suggests that selection of one method over others would not significantly alter the interpretation of the thermodynamics involved in HCCM pyrolysis. Similar findings have also been reported for studies related to cattle manure py-

rolysis, where enthalpies, entropies, and Gibbs free energies determined through multiple isoconversional models resulted in equivalent trends and magnitudes [26].

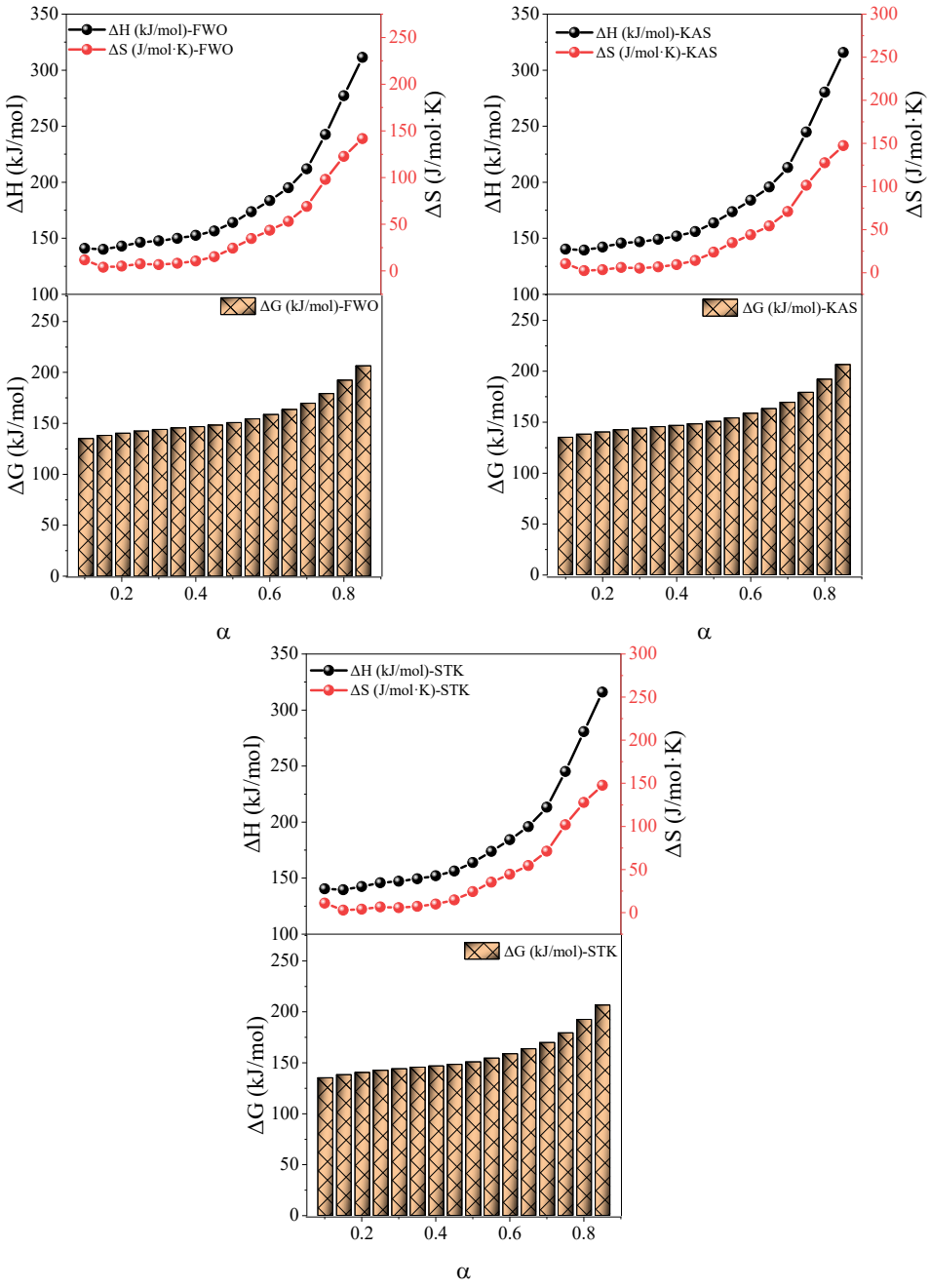


Figure 3. Thermodynamic parameters (ΔH, ΔS, and ΔG) of HCCM pyrolysis as a function of conversion (α).

Collectively, this evaluation suggests that HCCM pyrolysis represents an endothermic, non-spontaneous process in which activation complexes become increasingly disordered as conversion progresses. Furthermore, it suggests that the process requires additional energy input as conversion becomes greater, consistent with the increasing structural complexity and thermal stability of char-like products formed during hydrothermal carbonization.

3.5. TG-FTIR Analysis of Volatile Evolution During HCCM Pyrolysis

To determine the types of chemicals emitted as volatiles during HCCM pyrolysis and to connect these types to the various mass loss phases demonstrated in the TG-DTG

curves, the evolution of ten different infrared absorption peak intensities was determined through extraction from the online TG-FTIR spectra versus temperature (Figure 4): 2957, 2930, and 2871 cm^{-1}; 2357 cm^{-1}; 1740 and 1650 cm^{-1}; 1459 cm^{-1}; 1109 cm^{-1}; and 966 and 907 cm^{-1}. It has long been established that combining TG with FTIR allows researchers to track the real-time emission of gaseous and volatile products produced during biomass thermal decomposition, as well as link certain functional groups to specific phases of mass loss [13,34].

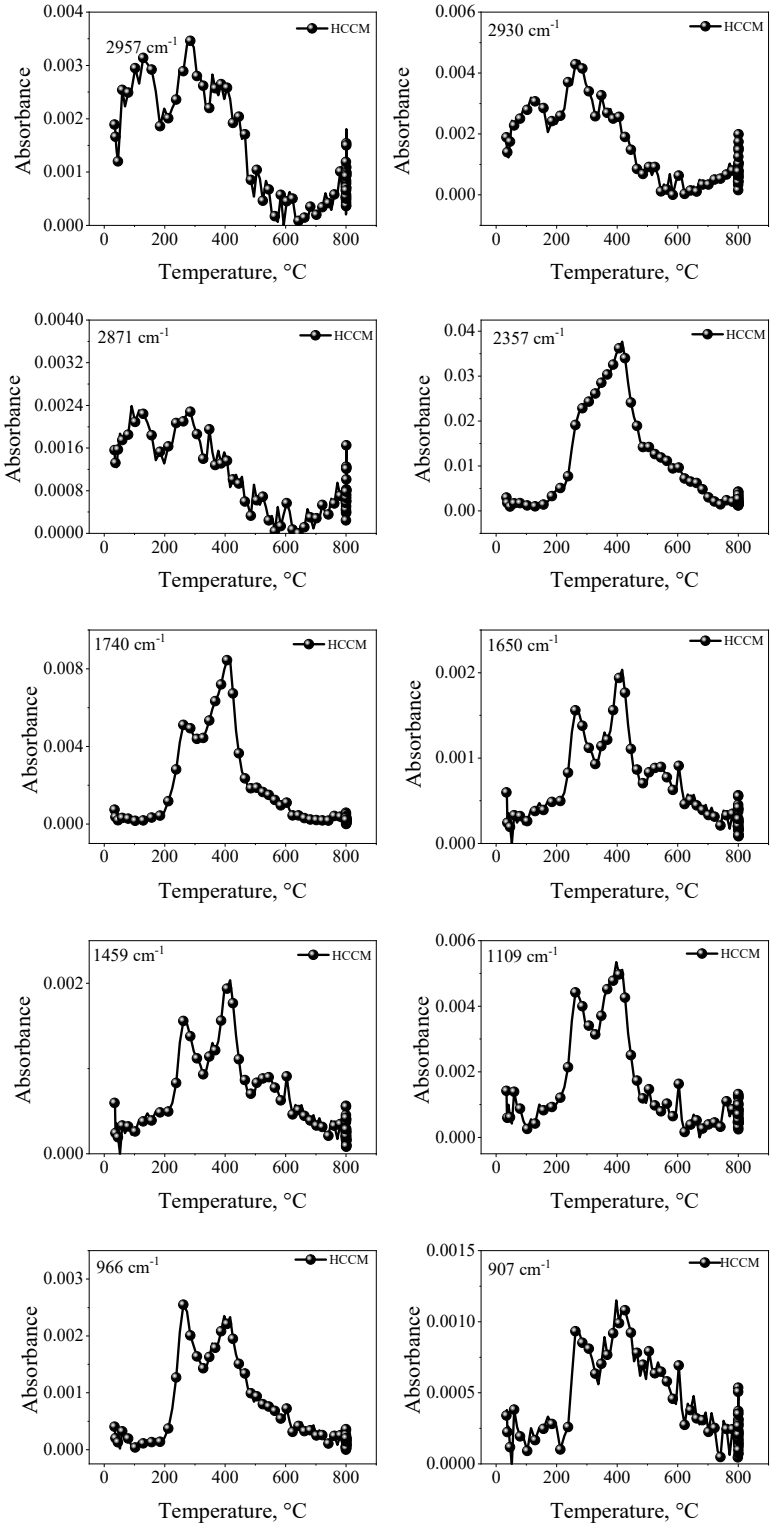


Figure 4. TG-FTIR infrared bands evolution characteristic of those released during HCCM pyrolysis.

It should be noted that, due to overlapping absorption bands and the possibility of secondary cracking, recombination, and re-condensation reactions occurring during pyrolysis, the assignment of specific IR bands to individual functional groups or reaction pathways should be regarded as tentative rather than definitive, consistent with the inherent limitations of evolved gas analysis techniques when applied to complex, multi-component biomass-derived matrices.

These three closely spaced bands located within the aliphatic C-H stretching region (approximately 2850–2960 cm^{-1}), correspond to the asymmetric and symmetric C-H stretching vibrations associated with aliphatic -CH_3 and -CH_2 groups. All three bands showed a wide-ranging evolutionary trend, rising in intensity beyond ~150 °C, peaking in absorbance within the 250–350 °C range, and declining thereafter toward 600 °C, with a second rise occurring within approximately 700–800 °C. This type of evolutionary pattern can be expected when lighter aliphatic hydrocarbon compounds and alkyl chain fragments are released through the cracking of remaining aliphatic side chains, fats, and carbohydrate-related structures in the hydrochar. Such processes are generally most active during the main devolatilization phase of both biomass and hydrochar pyrolysis [35].

The absorbance band centered at 2357 cm^{-1} corresponding to the asymmetric stretching vibration of CO_2 was found to have evolved with the greatest intensity among all ten bands investigated. In addition, it also exhibited the narrowest evolutionary profile. Its absorbance rose sharply past 150 °C and peaked near 350–400 °C before beginning to decline gradually to a low, stable baseline above 600 °C. This band is commonly cited as being one of the easiest to recognize characteristics in TG-FTIR spectra of biomass pyrolysis. As such, CO_2 stretching/bending vibrations dominate the wavenumber region between 2250 and 2450 cm^{-1} during the primary devolatilization phase [36]. The large amount of CO_2 emitted into the gas stream is primarily due to decarboxylation/decomposition reactions of carboxylic acid (-COOH) and carbonyl-containing structures (such as residual organic acids and possibly esters formed/preserved during hydrothermal carbonization).

The carbonyl stretching bands at 1740 cm^{-1} (associated with C=O stretching vibrations in aldehydes, ketones, and carboxylic/ester carbonyl groups) showed a large increase in absorbance from 300 to 450 °C. There was an association between the largest mass loss event observed via DTG and the temperature-dependent increase in the carbonyl stretching bands. Other researchers have also shown that bands near 1650–1850 cm^{-1} are primarily due to aldehyde/ketone compounds formed through degradation of cellulose/hemicellulose derived structures [36]. An adjacent band at 1650 cm^{-1} showed similar temperature dependence but can be better attributed to both C=C skeletal vibrations of aromatic olefinic structures and amide C=O stretching (amide I band), particularly pertinent for HCCM, whose ultimate analysis (Table 1) confirms a residual nitrogen content of 1.08 wt.% retained within the hydrochar structure following hydrothermal treatment, consistent with retained amide/protein-derived nitrogen functionality in HCCM itself, where the amide bond provides additional information about the decomposition of these residual nitrogen-containing groups [37]. As such, the simultaneous release of the amide-related bands along with carbonyls and other volatile species such as CO2 and aliphatic c-h, suggests that protein and carbohydrate components undergo simultaneous decomposition in the first pyrolytic thermal event of HCCM.

The band located at 1459 cm^{-1}, which represents asymmetric bending vibrations of CH_3/-CH_2-, and aromatic ring skeletal vibrations (C=C), displays similar temperature-dependent behavior to the two aforementioned bands. Specifically, the maximum absorption was found within the 300–450 °C range. A number of investigators have noted specific associations between bands in the 1650–1430 cm^{-1} spectral region and benzene ring skeletal vibrations that arise from pyrolysis of phenolic/aromatic species [13]. These data indicate

that both aromatic ring formation processes and aliphatic chain scissions occur with increasing significance as pyrolysis progresses past the point of initial devolatilization onset.

The C-O-C and C-O stretching band at 1109 cm^{-1} showed the highest total intensity of all ten measured bands. Additionally, it exhibited a very broad peak that spanned the majority of the 250–450 °C temperature range, which was concurrent with the major devolatilization stage. These results support those of prior tg-ftir investigations into pyrolysis of manures/biomass, where C-O-C functional groups were determined to be some of the primary volatile species released throughout the primary mass loss zone between 200 and 500 °C [35]. The lower frequency bands at 966 and 907 cm^{-1} represent the out-of-plane C-H bending typically seen as part of aromatic and olefinic structures (with possible overlap with N-H wagging modes relevant to nitrogenous compounds) and exhibited similar evolution profiles to the high-frequency bands, but peaked over the 300–450 °C temperature interval with a very small broadening of this peak above 700–800 °C. The presence of an identifiable absorption signal in these bands up to approximately 800 °C indicates that there is still some slow release of aromatic and heteroatom-containing fragments from the char matrix formed from condensation of volatile species in the latter portion of the pyrolysis process. These observations are consistent with the slow rate of mass loss observed in the third stage of the TG-DTG plots.

Each of the ten monitored wavenumbers showed remarkably consistent overall trends in volatility evolution profile shapes. Each band had essentially no absorbance prior to approximately 150 °C; then a rapid increase in absorbance and a single dominant peak occurred between about 250 and 450 °C. Following this peak, there was a decrease in absorbance, with a second, less prominent maximum occurring at temperatures slightly greater than 700–800 °C. The similarity between the shape of the FTIR evolution profiles and the DTG mass loss curve clearly demonstrates that most of the gaseous products (CO_2, light aliphatics, carbonyls and amides, ethers, aromatics) are released simultaneously during the first major volatilization stage of HCCM pyrolysis. The concurrent release of CO_2, hydrocarbon, oxygenated, and nitrogenous species during the first decomposition phase has also been documented previously for other types of manure- and protein-rich biomass substrates studied using TG-FTIR [38,39].

3.6. TG-MS Analysis of Gas-Phase Species Evolved During HCCM Pyrolysis

The combination of TG-FTIR and TG-MS provides an integrated approach to evolved gas analysis. With MS being able to detect both permanent gases and the lower molecular weight organic fragments through specific m/z values, it complements the structural–functional group information provided by FTIR. A number of researchers have used this method as a way to provide a complete characterization of the pyrolysis products [14,40].

Similarly, because several mass fragments can arise from more than one parent molecule or from secondary fragmentation/recombination reactions during ionization, the species assignments discussed below should be interpreted as the most probable identifications consistent with the observed m/z values and evolution profiles, rather than unambiguous structural confirmations.

The total ion current due to H_2 was very low until approximately 400 °C, at which point there was a sharp rise in intensity, reaching a large peak over a temperature interval between 500 °C and 700 °C, prior to decreasing towards 800 °C, as shown in Figure 5. The evolution profile of H_2 is representative of the secondary cracking and dehydrogenation/aromatization of the char matrix; specifically, after the majority of primary volatilization has occurred. This is in agreement with what has been found previously regarding the order of evolution of the pyrolysis products; H_2 is usually one of the last of the major pyrolysis products to evolve; i.e., H_2O, CO_2, CO, CH_4, and then finally H_2 [41]. The late

evolution of H_2 can be attributed to the gradual polymerization and condensation of aromatic rings into the char matrix, allowing the hydrogen atoms associated with these rings to become part of a more ordered and graphitic carbon structure.

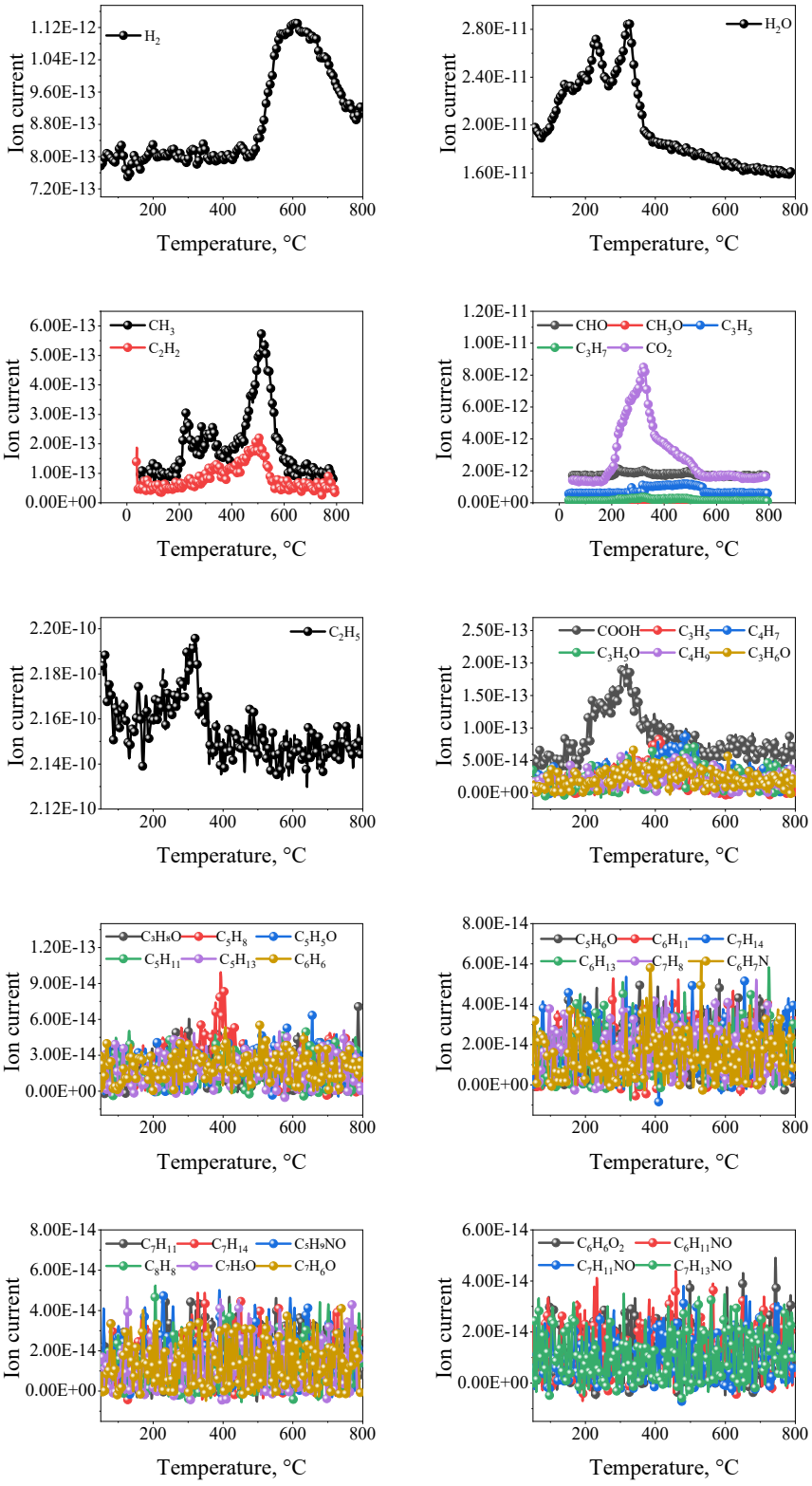


Figure 5. TG-MS ion-current evolution profiles of gas-phase species released during HCCM pyrolysis.

There are two overlapping peaks in the total ion current due to H_2O; each occurs in the temperature range of 200–350 °C. Following this region, there is a significant decrease in intensity, resulting in a baseline value approaching zero. The lower temperature peak is

thought to represent the evaporation of remaining physically and/or chemically bound water present on the surface or within the pores of the char material following hydrothermal carbonization. The second peak represents the dehydration reaction involving hydroxyl-, carboxyl-, and possibly other oxygen-containing functional groups present in the hydrocarbon structure as it undergoes primary thermal decomposition. It is commonly noted that water is produced early and often in greater quantity than all other volatile materials present in the product stream from pyrolysis of biomass and manure, and usually evolves prior to CO_2, CO, CH_4, and H_2 [41].

Ion current for the CH_3 and C_2H_2 fragments each had a major peak at a higher temperature than did H_2O, approximately 450–550 °C for the fragments, with CH_3 having the larger, broader signal. Such behavior is consistent with secondary cracking of pyrolytic tar and aliphatic side chains into light hydrocarbon radicals and fragments, which are generally enhanced after the initial volatiles have been removed; acetylene (C_2H_2), in particular, has often been identified as a result of secondary reactions through recombination and cracking at elevated temperatures during pyrolysis [40].

Of these six plotted species, CO_2 produced the largest, sharpest signal, with its single peak occurring in the 300–400 °C range, nearly simultaneously with the maximum rate of mass loss and with the appearance of the 2357 cm^{-1} CO_2 absorption band in the TG-FTIR spectrum. In contrast, the oxygen-containing fragments CHO, CH_3O, C_3H_5, and C_3H_7 produced lower-intensity, more horizontal signals over the entire temperature range, indicating that each represented only small amounts of fragment species. A similar profile, an intense CO_2 signal peaking at a narrow range of temperatures along with weak signals from related oxygenated fragments, is typical of decarboxylation and decarbonylation reactions that occur during the primary pyrolysis stage when carboxyl and carbonyl groups are broken down; CO_2 is a commonly reported major gas-phase product of manure pyrolysis [39].

The C_2H_5 ion current remained nearly flat and noisy across all temperature ranges, with only a faint, broad increase around 200–350 °C. Thus, it appears that ethyl fragments were present at very low concentration levels and largely independent of temperature rather than as part of a defined decomposition process.

Carboxylic acid and mixed oxygen-containing fragments (COOH, C_2H_3, C_2H_7, C_2H_5O, C_4H_5, C_3H_4O). The COOH fragment displayed the strongest trend among the members of this group, reaching a broad maximum at 200–300 °C prior to gradually declining. This is consistent with the thermal degradation of carboxylic acids at relatively low pyrolysis temperatures, a phase preceding the stronger CO_2 release due to further deepening decarboxylation of char. As previously noted for other members of this group (C_2H_3, C_2H_7, C_2H_5O, C_4H_5, C_3H_4O), those present here also presented weak, non-descript traces indicative of the presence of minor co-evolving species.

The heavier, nitrogen containing (C_5-C_7 hydrocarbons and N-heterocyclic fragments) fragments from the mass were monitored (C_5H_8O, C_3H_8, C_2H_3O, C_5H_{11}, C_2H_{13}, C_6H_6, C_3H_4O, C_4H_{11}, C_3H_{14}, C_4H_{12}, C_7H_5, C_6H_7N, C_7H_{11}, C_7H_{14}, C_4H_5NO, C_3H_8, C_4H_7O, C_6H_4O, $C_6H_4O_2$, $C_6H_{11}NO$, $C_5H_{11}NO$ and $C_6H_{12}NO$). All of these other mass fragments displayed very weak/noisy ion current profiles with no distinct peaks resolved; they continued to fluctuate near the instrument's baseline throughout the pyrolysis experiment. Although each of these fragments was individually minor, it is worth noting that several of them contained nitrogen (i.e., C_6H_7N, C_4H_5NO, $C_6H_{11}NO$, $C_5H_{11}NO$ and $C_6H_{12}NO$), consistent with the residual nitrogen retained within the HCCM structure itself following hydrothermal treatment (1.08 wt.%, Table 1), rather than reflecting the substantially higher nitrogen content of the untreated raw manure feedstock (3.83 wt.%). These nitrogen-containing species would be expected to derive from traces of nitrogen-heterocyclic and

amide/amine-derived tars that have been shown to be produced during pyrolysis of protein rich manures/sewage derived biomass [39,42]. This is consistent with the substantially depleted solid-phase nitrogen pool established in Section 3.1, where the majority of the original chicken manure nitrogen (3.83 wt.%) was solubilized into the aqueous phase during hydrothermal treatment, leaving only 1.08 wt.% retained in HCCM [17,18]. The low-intensity nitrogen-containing MS fragments observed here therefore reflect pyrolytic release of this smaller, more recalcitrant residual nitrogen fraction, rather than the full nitrogen inventory of the original feedstock. Due to their small and erratic signal intensities compared to the major species (H_2O, CO_2, CH_3, and H_2), it appears that HCCM produces its nitrogen as trace levels of heavy fragments or as some other species not being detected by the specific m/z channels monitored (e.g., ammonia or hydrogen cyanide).

The overall trend revealed by TG-MS analysis is a clear temporal relationship among gas species based on their respective release times corresponding to the staged degradation process identified in TG-DTG and TG-FTIR experiments: at relatively lower temperatures, water and acidic carbonyl fragments are evolved first; between 250 °C and 400 °C, CO_2 and lighter oxygenates make up the majority of the primary thermal decomposition stage; and at higher temperatures, lighter hydrocarbons (CH_3, C_2H_2) along with H_2 are evolved as a result of subsequent cracking/aromatization and charring processes occurring until ~800 °C. Overall, this sequential release pattern (water and CO_2 precede the evolution of hydrocarbons/H_2) is generally similar to gas evolution orders found in prior TG-MS studies involving manure/biomass pyrolysis [39,41].

3.7. Proposed Reaction Mechanism of HCCM Pyrolysis

Evidence from all of the analytical techniques used, including TG-DTG; isoconversion kinetics (FWO/KAS/STK); thermodynamics; TG-FTIR, and TG-MS, indicates that it is possible to propose a reaction mechanism for the thermal degradation of HCCM as shown in Figure 6. The initial hydrochar is itself a result of hydrothermal carbonization. During this process, the raw chicken manure undergoes hydrolysis, dehydration, decarboxylation, and polymerization/aromatization, in part under subcritical water conditions. As a result of these processes, a carbon-rich material remains, having some residual oxygen-/nitrogen-containing functionalities as well as significantly reduced hemicellulose content compared to the original feedstock [8,43]. These factors help explain why there is no discernible low-temperature hemicellulose shoulder present in the HCCM DTG plots.

Pyrolysis of HCCM occurs over three sequential steps. Between approximately 50 °C and 150 °C, the last remaining moisture and weakly held water are evolved. Over the temperature range of 180–400 °C, which represents the majority of the volatile release step, significant amounts of water vapor and carbon dioxide gas are evolved concurrently. A number of infrared absorption peaks were also observed simultaneously, corresponding to carbonyl-/amide-related frequencies (1740 and 1650 cm^{-1}) and the C-O-C stretching frequency (1109 cm^{-1}). In addition, small amounts of nitrogen-containing mass spectral fragments indicative of depolymerization of residual protein/polysaccharide structures were also detected [10,37].

Above 400 °C, the slow evolution of light hydrocarbons (CH_3, C_2H_2) and most notably hydrogen gas (peaking between 500 and 700 °C) reflects secondary fragmentation of the evolving tar/aliphatic side chains occurring through dehydrogenation and aromatization/condensation reactions in the growing char. Ultimately, hydrogen and aromatic species are expelled while a thermally stable, graphite-like char structure develops [12].

This staged pathway is also supported by kinetic and thermodynamic data: the apparent activation energies and enthalpies increase with increasing conversion (from approximately 150 to approximately 320 KJ/mol over FWO, KAS, and STK) likely reflecting

a transition from the relatively facile breakdown of carbohydrate and protein fragments at low conversion to a combination of mineral/ash-catalyzed effects and the increased thermal stability of condensed aromatic char structures formed during hydrothermal carbonization at high conversion, with the relative contribution of each mechanism not distinguishable from the present dataset. The correspondingly positive and increasing Gibbs free energy of activation (ΔG) reflects a progressively greater energy barrier to decomposition and increased resistance to the reaction proceeding at higher conversion levels, rather than indicating that the overall pyrolysis reaction is thermodynamically non-spontaneous; the positive ΔH values separately confirm that the reaction is endothermic and requires continued heat input to proceed, whereas the continuously increasing entropy at higher conversions indicates a larger degree of randomness within the activated complexes resulting from further aromatization [16,32].

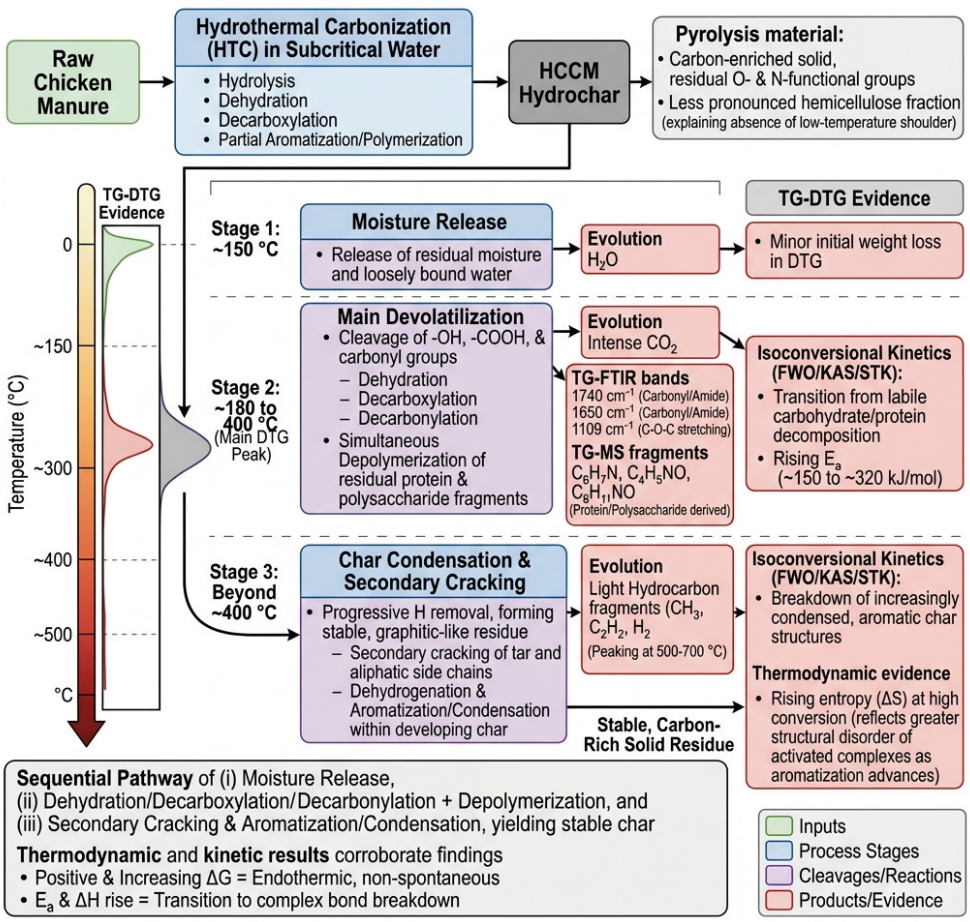


Figure 6. Proposed reaction mechanism of the HCCM pyrolysis.

Thus, overall, this sequence may be represented as a three-step pathway consisting of: (i) moisture loss; (ii) dehydration, decarboxylation, decarbonylation and depolymerization of the remaining carbohydrate and protein residues; and (iii), secondary cracking aromatization/condensation of the char, resulting in a final product of a highly carbon rich solid residue—consistent with previously reported reaction schemes for both hydrothermal carbonization, and thermal degradation/pyrolysis of manure-derived biomass [10,44].

4. Conclusions

The study provided an extensive overview of the pyrolytic characteristics of hydrochar derived from chicken manure (HCCM). TG-DTG, TG-FTIR, TG-MS, isoconversional kinetics, and thermodynamics were used to provide a complete description of HCCM. Three

different stages were observed in TG-DTG for the decomposition of HCCM moisture evaporation occurring below 150 °C; a major devolatilization stage between 180 and 400 °C; and a minor carbonization stage continuing up to 800 °C, which produced a residual char material weighing approximately 22–27 wt.% of the original sample. The maximum rate of decomposition was significantly affected by an increase in heating rate from 5 to 25 °C/min. Also, an increase in heating rate resulted in the shifting of the DTG peak to occur at a higher temperature, providing additional evidence that pyrolysis of HCCM is a kinetically controlled and heat transfer-controlled process. Consistent activation energy profiles ($R^2 > 0.98$) were obtained using the FWO, KAS, and Starink isoconversional kinetic methods. Activation energies ranged from ~150 kJ/mol at lower conversions to over 320 kJ/mol at higher conversions, likely reflecting a transition from the breakdown of labile carbohydrate/protein-based fragments at low conversion to a combination of mineral/ash-catalyzed effects and the degradation of increasingly condensed aromatic char structures at high conversion, with the relative contribution of each mechanism not distinguishable from the present dataset. Thermodynamic calculations also indicated that HCCM pyrolysis is an endothermic process, as evidenced by the consistently positive ΔH values, with the correspondingly positive and increasing Gibbs free energy of activation (ΔG) reflecting a progressively greater energy barrier to decomposition and thus increased resistance to the reaction proceeding at higher conversion levels, rather than indicating that the overall pyrolysis reaction is thermodynamically non-spontaneous. Additional information regarding volatile production during pyrolysis was gathered using TG-FTIR and TG-MS. Dominant species evolved during the main devolatilization phase included CO_2, H_2O, carbonyl/amide-related fragments, and light aliphatic hydrocarbons. Delayed appearance of H_2 at elevated temperatures suggested secondary cracking, dehydrogenation, and aromatization/condensation reactions within the evolving char matrix.

Nitrogen-containing fragments were identified throughout the entire pyrolysis process, consistent with the residual nitrogen retained within the HCCM structure itself following hydrothermal treatment (1.08 wt.%). Collectively, these data support a proposed mechanistic framework of sequential dehydration, decarboxylation, decarbonylation, and aromatization/condensation reactions as a plausible interpretation of the HCCM pyrolysis process, consistent with the tentative nature of the FTIR/MS species assignments. These data show that this hydrochar is expected to undergo a thermally driven transformation into a carbon-rich residue. Isoconversional methods produced similar kinetic and thermodynamic parameters, thus lending credibility to these results and establishing a strong foundation for designing pyrolysis reactor systems optimized for chicken manure-based hydrochar. Further research should focus on examining product yields (bio-oil, biochar, syngas composition) as well as testing the proposed mechanistic framework through Py-GC/MS experiments and demineralization studies to isolate the relative contributions of mineral/ash-catalyzed effects versus aromatic char structure to the observed activation energy trends, in order to further assess the feasibility of utilizing HCCM as a renewable solid fuel source within a circular waste-to-energy model.

Supplementary Materials: The following supporting information can be downloaded at: https://www.mdpi.com/article/10.3390/biomass6050070/s1, Table S1: Effect of heating rate on the thermal decomposition parameters expressed as mean ± SD.

Author Contributions: A.K.; Conceptualization, methodology, software, writing—review and editing, writing original draft preparation; L.K.; validation, writing—review and editing; M.A.A.; formal analysis, writing—review and editing; B.T.O.; writing—review and editing, Q.M.; visualization, Q.Z.; supervision; project administration; funding acquisition. All authors have read and agreed to the published version of the manuscript.

Funding: This research is financially supported by the Key Techniques for Improving the Quality of Cultivated Land and Rehabilitating Degraded Land in Shanxi Province (202201140601028).

Data Availability Statement: The original contributions presented in this study are included in the article/supplementary material. Further inquiries can be directed to the corresponding author.

Conflicts of Interest: The authors declare no conflicts of interest.

References

1. Rahman Alvi, K.M.; Mondal, S. Ammonia & CO_2 Gas Detection of Poultry Farms and Compost Plants by Low-Cost Smart Sensing System. In Proceedings of the 2023 26th International Conference on Computer and Information Technology (ICCIT), Cox's Bazar, Bangladesh, 13–15 December 2023; pp. 1–6.
2. Sanchez-Silva, J.M.; Ocampo-Pérez, R.; Padilla-Ortega, E.; Sangaré, D.; Escobedo-Bretado, M.A.; Domínguez-Arvizu, J.L.; Hernández-Majalca, B.C.; Salinas-Gutiérrez, J.M.; López-Ortiz, A.; Collins-Martínez, V. Pyrolysis Kinetics of *Byrsonima crassifolia* Stone as Agro-Industrial Waste through Isoconversional Models. *Molecules* **2023**, *28*, 544. [CrossRef] [PubMed]
3. Kacprzak, M.; Malińska, K.; Grosser, A.; Sobik-Szołtysek, J.; Wystalska, K.; Dróżdż, D.; Jasińska, A.; Meers, E. Cycles of Carbon, Nitrogen and Phosphorus in Poultry Manure Management Technologies—Environmental Aspects. *Crit. Rev. Environ. Sci. Technol.* **2023**, *53*, 914–938. [CrossRef]
4. Cha, R.; Kumar, V.; Singh, J.; Sharma, N. Poultry Manure and Poultry Waste Management: A Review. *Int. J. Curr. Microbiol. App. Sci.* **2020**, *9*, 3483–3495. [CrossRef]
5. Boakye-Yiadom, K.A.; Ilari, A.; Bisinella, V.; Duca, D. Environmental Impact of Poultry Manure Gasification Technology for Energy and Ash Valorization. *Sustainability* **2024**, *16*, 9941. [CrossRef]
6. Ipiales, R.P.; de la Rubia, M.A.; Diaz, E.; Mohedano, A.F.; Rodriguez, J.J. Integration of Hydrothermal Carbonization and Anaerobic Digestion for Energy Recovery of Biomass Waste: An Overview. *Energy Fuels* **2021**, *35*, 17032–17050. [CrossRef]
7. Devnath, B.; Khanal, S.; Shah, A.; Reza, T. Hydrochar and Biochar from Dairy Manure as Stable Carbon Amendments for Greenhouse Gas Mitigation and Carbon Sequestration in Concentrated Animal Feeding Operations. *Environ. Res. Commun.* **2026**, *8*, 65015. [CrossRef]
8. Durak, H.; Yarbay, R.Z.; Atilgan Türkmen, B. Hydrothermal Carbonization of Biomass for Hydrochar Production: Mechanisms, Process Parameters, and Sustainable Valorization. *Processes* **2026**, *14*, 339. [CrossRef]
9. Marin-Batista, J.D.; Villamil, J.A.; Qaramaleki, S.V.; Coronella, C.J.; Mohedano, A.F.; de la Rubia, M.A. Energy Valorization of Cow Manure by Hydrothermal Carbonization and Anaerobic Digestion. *Renew. Energy* **2020**, *160*, 623–632. [CrossRef]
10. Song, E.; Park, S.; Han, S.; Lee, E.; Kim, H. Characteristics of Hydrothermal Carbonization Hydrochar Derived from Cattle Manure. *Energies* **2022**, *15*, 9195. [CrossRef]
11. Zhang, Z.; Li, Y.; Luo, L.; Yellezuome, D.; Rahman, M.M.; Zou, J.; Hu, H.; Cai, J. Insight into Kinetic and Thermodynamic Analysis Methods for Lignocellulosic Biomass Pyrolysis. *Renew. Energy* **2023**, *202*, 154–171. [CrossRef]
12. Nadarajah, K.; Asharp, T.; Jeganathan, Y. Biochar from Waste Biomass, Its Fundamentals, Engineering Aspects, and Potential Applications: An Overview. *Water Sci. Technol.* **2024**, *89*, 1211–1239. [CrossRef] [PubMed]
13. Zhang, J.; Sekyere, D.T.; Niwamanya, N.; Huang, Y.; Barigye, A.; Tian, Y. Study on the Staged and Direct Fast Pyrolysis Behavior of Waste Pine Sawdust Using High Heating Rate TG-FTIR and Py-GC/MS. *ACS Omega* **2022**, *7*, 4245–4256. [CrossRef] [PubMed]
14. Christensen, E.; Evans, R.J.; Carpenter, D. High-Resolution Mass Spectrometric Analysis of Biomass Pyrolysis Vapors. *J. Anal. Appl. Pyrolysis* **2017**, *124*, 327–334. [CrossRef]
15. Arenas, C.N.; Navarro, M.V.; Martínez, J.D. Pyrolysis Kinetics of Biomass Wastes Using Isoconversional Methods and the Distributed Activation Energy Model. *Bioresour. Technol.* **2019**, *288*, 121485. [CrossRef] [PubMed]
16. Zhai, M.; Guo, L.; Zhang, Y.; Dong, P.; Qi, G.; Huang, Y. Kinetic Parameters of Biomass Pyrolysis by TGA. *BioResources* **2016**, *11*, 8548–8557. [CrossRef]
17. Zong, C.; Belete, Y.Z.; Das, A.K.; Chen, L. Effects of Operating Conditions on Nitrogen Recovery from Post-Hydrothermal Carbonization Liquids Using Gas-Permeable Membranes. *ChemEngineering* **2026**, *10*, 96. [CrossRef]
18. Huang, H.; Su, Q.; Li, J.; Niu, Z.; Wang, D.; Wei, C.; Long, S.; Ren, J.; Wang, J.; Shan, B.; et al. Effects of Process Water Obtained from Hydrothermal Carbonization of Poultry Litter on Soil Microbial Community, Nitrogen Transformation, and Plant Nitrogen Uptake. *J. Environ. Manag.* **2022**, *323*, 116307. [CrossRef] [PubMed]
19. Pu, X.; Wei, M.; Chen, X.; Wang, L.; Deng, L. Thermal Decomposition Characteristics and Kinetic Analysis of Chicken Manure in Various Atmospheres. *Agriculture* **2022**, *12*, 607. [CrossRef]
20. Devnath, B.; Khanal, S.; Shah, A.; Reza, T. Influence of Hydrothermal Carbonization (HTC) Temperature on Hydrochar and Process Liquid for Poultry, Swine, and Dairy Manure. *Environments* **2024**, *11*, 150. [CrossRef]

21. Portilla-Amaguaña, A.; Barraza-Burgos, J.; Guerrero-Perez, J.; Borugadda, V.B.; Dalai, A.K. Combustion Reactivity of Hydrochars Derived from Sugarcane Green Harvesting Residues via Hydrothermal Carbonization. *BioEnergy Res.* **2025**, *18*, 97. [CrossRef]
22. Gao, Y.; Yu, B.; Wu, K.; Yuan, Q.; Wang, X.; Chen, H. Physicochemical, Pyrolytic, and Combustion Characteristics of Hydrochar Obtained by Hydrothermal Carbonization of Biomass. *BioResources* **2016**, *11*, 4113–4133. [CrossRef]
23. Gonnella, G.; Ischia, G.; Fambri, L.; Fiori, L. Thermal Analysis and Kinetic Modeling of Pyrolysis and Oxidation of Hydrochars. *Energies* **2022**, *15*, 950. [CrossRef]
24. Gu, J.; Chong, C.T.; Mong, G.R.; Ng, J.-H.; Chong, W.W.F. Determination of Pyrolysis and Kinetics Characteristics of Chicken Manure Using Thermogravimetric Analysis Coupled with Particle Swarm Optimization. *Energies* **2023**, *16*, 1919. [CrossRef]
25. Yuan, X.; He, T.; Cao, H.; Yuan, Q. Cattle Manure Pyrolysis Process: Kinetic and Thermodynamic Analysis with Isoconversional Methods. *Renew. Energy* **2017**, *107*, 489–496. [CrossRef]
26. Gajera, B.; Tyagi, U.; Sarma, A.K.; Jha, M.K. Pyrolysis of Cattle Manure: Kinetics and Thermodynamic Analysis Using TGA and Artificial Neural Network. *Biomass Convers. Biorefin.* **2024**, *14*, 23605–23621. [CrossRef]
27. Padma, D.V.; Kumar, K.R.; Sastry, S.V.A.R.; Barmavatu, P. Studies on Thermal Degradation Kinetics and Machine Learning Modeling of Hydrochar Produced from Hydrothermal Carbonization of Municipal Sewage Sludge and Key Lime Peel. *Biomass Convers. Biorefin.* **2025**, *15*, 26385–26400. [CrossRef]
28. Xu, Y.; Chen, B. Investigation of Thermodynamic Parameters in the Pyrolysis Conversion of Biomass and Manure to Biochars Using Thermogravimetric Analysis. *Bioresour. Technol.* **2013**, *146*, 485–493. [CrossRef] [PubMed]
29. Carrier, M.; Auret, L.; Bridgwater, A.; Knoetze, J.H. Using Apparent Activation Energy as a Reactivity Criterion for Biomass Pyrolysis. *Energy Fuels* **2016**, *30*, 7834–7841. [CrossRef]
30. Vyazovkin, S. Misinterpretation of Thermodynamic Parameters Evaluated from Activation Energy and Preexponential Factor Determined in Thermal Analysis Experiments. *Thermo* **2024**, *4*, 373–381. [CrossRef]
31. Tibola, F.L.; de Oliveira, T.J.P.; Ataíde, C.H.; Cerqueira, D.A.; Sousa, N.G.; Cardoso, C.R. Temperature-Programmed Pyrolysis of Sunflower Seed Husks: Application of Reaction Models for the Kinetic and Thermodynamic Calculation. *Biomass Convers. Biorefin.* **2023**, *13*, 13841–13858. [CrossRef]
32. Fischer, O.; Lemaire, R.; Bensakhria, A. Thermogravimetric Analysis and Kinetic Modeling of the Pyrolysis of Different Biomass Types by Means of Model-Fitting, Model-Free and Network Modeling Approaches. *J. Therm. Anal. Calorim.* **2024**, *149*, 10941–10963. [CrossRef] [PubMed]
33. Slopiecka, K.; Bartocci, P.; Fantozzi, F. Thermogravimetric Analysis and Kinetic Study of Poplar Wood Pyrolysis. *Appl. Energy* **2012**, *97*, 491–497. [CrossRef]
34. Shen, J.; Liu, J.; Xing, Y.; Zhang, H.; Luo, L.; Jiang, X. Application of TG-FTIR Analysis to Superfine Pulverized Coal. *J. Anal. Appl. Pyrolysis* **2018**, *133*, 154–161. [CrossRef]
35. Yang, J.; Wang, H.; Huang, W.; Peng, X.; Yuan, B.; Hu, Y. TG-FTIR-MS and Py-GC/MS Study on the Pyrolysis Characteristics and Gas Evolution Behavior of Forest Duff. *J. Anal. Appl. Pyrolysis* **2023**, *176*, 106233. [CrossRef]
36. Apaydın Varol, E.; Mutlu, Ü. TGA-FTIR Analysis of Biomass Samples Based on the Thermal Decomposition Behavior of Hemicellulose, Cellulose, and Lignin. *Energies* **2023**, *16*, 3674. [CrossRef]
37. Schnitzer, M.I.; Monreal, C.M.; Facey, G.A.; Fransham, P.B. The Conversion of Chicken Manure to Biooil by Fast Pyrolysis I. Analyses of Chicken Manure, Biooils and Char by 13C and 1H NMR and FTIR Spectrophotometry. *J. Environ. Sci. Health Part B* **2007**, *42*, 71–77. [CrossRef] [PubMed]
38. Giuntoli, J.; de Jong, W.; Arvelakis, S.; Spliethoff, H.; Verkooijen, A.H.M. Quantitative and Kinetic TG-FTIR Study of Biomass Residue Pyrolysis: Dry Distiller's Grains with Solubles (DDGS) and Chicken Manure. *J. Anal. Appl. Pyrolysis* **2009**, *85*, 301–312. [CrossRef]
39. Zhang, J.; Liu, J.; Evrendilek, F.; Zhang, X.; Buyukada, M. TG-FTIR and Py-GC/MS Analyses of Pyrolysis Behaviors and Products of Cattle Manure in CO_2 and N_2 Atmospheres: Kinetic, Thermodynamic, and Machine-Learning Models. *Energy Convers. Manag.* **2019**, *195*, 346–359. [CrossRef]
40. Radojević, M.; Janković, B.; Stojiljković, D.; Jovanović, V.; Čeković, I.; Manić, N. Improved TGA-MS Measurements for Evolved Gas Analysis (EGA) during Pyrolysis Process of Various Biomass Feedstocks. Syngas Energy Balance Determination. *Thermochim. Acta* **2021**, *699*, 178912. [CrossRef]
41. Ma, M.; Bai, Y.; Song, X.; Wang, J.; Su, W.; Yao, M.; Yu, G. Investigation into the Co-Pyrolysis Behaviors of Cow Manure and Coal Blending by TG–MS. *Sci. Total Environ.* **2020**, *728*, 138828. [CrossRef] [PubMed]
42. Fan, M.; Xing, N.; Zhu, J.; Zhang, X.; Chen, Y.; Wang, G.; Wang, X.; Pan, Z.; Embaye, T.M. TG-FTIR-MS and Py-GC/MS Analysis on Co-Pyrolysis Characteristics of Municipal Solid Waste and Sewage Sludge. *J. Energy Inst.* **2026**, *125*, 102448. [CrossRef]

43. Tihin, G.L.; Mo, K.H.; Onn, C.C.; Ong, H.C.; Taufiq-Yap, Y.H.; Lee, H.V. Overview of Municipal Solid Wastes-Derived Refuse-Derived Fuels for Cement Co-Processing. *Alex. Eng. J.* **2023**, *84*, 153–174. [CrossRef]
44. Yang, J.; Zhang, Z.; Wang, J.; Zhao, X.; Zhao, Y.; Qian, J.; Wang, T. Pyrolysis and Hydrothermal Carbonization of Biowaste: A Comparative Review on the Conversion Pathways and Potential Applications of Char Product. *Sustain. Chem. Pharm.* **2023**, *33*, 101106. [CrossRef]

Disclaimer/Publisher's Note: The statements, opinions and data contained in all publications are solely those of the individual author(s) and contributor(s) and not of MDPI and/or the editor(s). MDPI and/or the editor(s) disclaim responsibility for any injury to people or property resulting from any ideas, methods, instructions or products referred to in the content.